remote sensing

MDPI

Article

Tracking Post-Fire Vegetation Regrowth and Burned Areas Using Bitemporal Sentinel-1 SAR Data: A Google Earth Engine Approach in Heath Vegetation of Mooloolah River National Park, Queensland, Australia

Harikesh Singh [1,2], Prashant K. Srivastava [1,3], Rajendra Prasad [4] and Sanjeev Kumar Srivastava [1,*]

[1] Geospatial Analytics for Conservation & Management, School of Science Engineering and Technology, University of the Sunshine Coast, Maroochydore, QLD 4558, Australia; harikesh@research.usc.edu.au (H.S.); psrivastava@usc.edu.au (P.K.S.)
[2] SmartSat Cooperative Research Centre, North Terrace, Adelaide, SA 5000, Australia
[3] Remote Sensing Laboratory, Institute of Environment and Sustainable Development, Banaras Hindu University, Varanasi 221005, India
[4] Department of Physics, Indian Institute of Technology (BHU), Varanasi 221005, India; rprasad.app@itbhu.ac.in
* Correspondence: ssrivast@usc.edu.au

Abstract: This study utilizes the unique capabilities of Sentinel-1 C-band synthetic aperture radar (SAR) data to map post-fire burned areas and monitor vegetation recovery in a heath-dominated Queensland National Park. Sentinel-1 SAR data were used due to their cloud-penetrating capability and frequent revisit times. Using Google Earth Engine (GEE), a bitemporal ratio analysis was applied to SAR data from post-fire periods between 2021 and 2023. SAR backscatter changes over time captured fire impacts and subsequent vegetation regrowth. This differentiation was further enhanced with k-means clustering. Validation was supported by Sentinel-2 dNBR and official fire history records. The dNBR provided a quantitative assessment of burn severity and was used alongside the fire history data to evaluate the accuracy of the burned area classification. While Sentinel-2 false-colour composite (FCC) imagery was generated for visualisation and interpretation purposes, the primary validation relied on dNBR and QPWS fire history records. The results highlighted significant vegetation regrowth, with some areas returning to near pre-fire biomass levels by March 2023. This approach demonstrates the sensitivity of Sentinel-1 SAR, especially in VV polarization, for detecting subtle changes in vegetation, providing a cost-effective method for post-fire ecosystem monitoring and informing ecological management strategies amid increasing wildfire events.

Keywords: Sentinel-1 SAR; bitemporal ratio analysis; post-fire vegetation recovery; Google Earth Engine (GEE); burned area mapping; vegetation regrowth; synthetic aperture radar (SAR)

Academic Editor: Ioannis Gitas

Received: 2 April 2025
Revised: 27 May 2025
Accepted: 11 June 2025
Published: 12 June 2025

Citation: Singh, H.; Srivastava, P.K.; Prasad, R.; Srivastava, S.K. Tracking Post-Fire Vegetation Regrowth and Burned Areas Using Bitemporal Sentinel-1 SAR Data: A Google Earth Engine Approach in Heath Vegetation of Mooloolah River National Park, Queensland, Australia. *Remote Sens.* **2025**, *17*, 2031. https://doi.org/10.3390/rs17122031

1. Introduction

Wildfires play a significant ecological role in shaping the structure and composition of vegetation communities, particularly in fire-adapted ecosystems such as Australia [1–3]. However, in recent decades, the frequency, intensity, and spatial extent of wildfires have increased globally due to the compounding effects of climate change, extended droughts, land-use change, and human activities [4,5]. These changes have intensified the impact of fires on biodiversity, ecosystem services, and carbon storage, thereby necessitating effective and timely post-fire monitoring strategies [6–9]. The accurate tracking of vegetation

recovery after fire events is essential to evaluate ecological resilience, inform management decisions, and guide restoration efforts [10–13].

Remote sensing has become an essential tool in wildfire research [12,14], offering the ability to assess fire impacts and vegetation regrowth across large spatial and temporal scales. Traditionally, optical remote sensing platforms such as Landsat and Sentinel-2 have been widely employed to evaluate fire severity and post-fire vegetation dynamics using spectral indices like the Normalized Burn Ratio (NBR) and differenced NBR (dNBR) [15–19]. While these sensors provide valuable information, their performance is often limited in post-fire environments due to the presence of clouds, smoke, and shadows that obscure surface reflectance data [20–22]. This limitation is particularly critical in regions with frequent cloud cover or during the immediate aftermath of fire events.

Synthetic aperture radar (SAR) sensors, operating in the microwave domain, offer a viable alternative to optical sensors due to their ability to penetrate clouds and smoke and to capture data under all weather conditions and during both day and night [23]. Sentinel-1, a C-band SAR mission under the Copernicus program, provides regular, high-resolution SAR data with dual polarization, making it highly suitable for monitoring structural and moisture-related changes in vegetation [24,25]. SAR backscatter is sensitive to variations in vegetation structure, water content, and surface roughness, enabling the detection of subtle changes associated with both fire damage and subsequent regrowth [26–29]. These attributes make SAR particularly effective for monitoring ecosystems where early vegetation recovery may not be spectrally prominent but can still be detected through structural changes [30–32].

In recent years, several studies have utilised SAR data to detect burned areas and assess vegetation regrowth [33–35]. While many of these studies focus on forested regions in temperate [36], Mediterranean climates [28] or boreal ecosystems [37], there is limited research addressing fire recovery in heathland and sclerophyll-dominated ecosystems [12]. Heathlands are understudied in SAR-based fire monitoring despite their ecological sensitivity. See the Study Area section for the full ecological context [38–40]. The heathland ecosystems, in particular, may require two to five years or more to return to pre-fire conditions, depending on species composition, soil moisture, and climatic variability [41].

While SAR has been widely applied for post-fire mapping in forested and agricultural landscapes, its application in low-stature ecosystems such as heathlands is limited. These ecosystems pose challenges for remote sensing due to their structural complexity and slow regrowth, which may not be easily detected by conventional optical or SAR methods. Addressing this gap, the present study explores SAR-based fire recovery monitoring in a heath-dominated national park using a scalable and unsupervised approach. This study applies a bitemporal Sentinel-1 SAR ratio analysis approach to detect burned areas and assess vegetation recovery without relying on ground-truth or training datasets. The use of bitemporal ratios minimises the influence of seasonal and environmental variability, focusing on proportional changes caused by fire disturbance and regrowth [42–44]. The entire analysis is implemented using Google Earth Engine (GEE), a cloud-based geospatial processing platform that allows for the scalable and efficient handling of large Earth observation datasets [45,46]. In addition, the integration of Sentinel-1 SAR processing within the Google Earth Engine (GEE) platform enables the efficient, cloud-based automation of large-scale analysis. This approach improves replicability and operational monitoring, especially in regions where access to in situ data or high-performance computing is limited. By focusing on a heath- and sclerophyll-dominated ecosystem in Mooloolah River National Park, Queensland, this study demonstrates the utility of SAR-based change detection for fire monitoring in underrepresented vegetation types and highlights the value of cloud-based platforms for automated, repeatable analyses.

In addition, this study addresses a key gap in the current literature by evaluating the performance of SAR-based methods in detecting varying stages of regrowth in non-forest ecosystems. Previous work has largely focused on forests, with limited attention to fire recovery in other ecosystems. The use of Sentinel-1 C-band SAR data allows for frequent and consistent observations of the fire-affected area, enabling the capture of both immediate and longer-term recovery signals [47–50]. The results are compared with the Queensland Parks and Wildlife Service (QPWS) fire history dataset, which provides authoritative fire perimeter polygons derived from satellite imagery interpretation, field observations, and incident reports [14,51,52]. This dataset, typically mapped at a scale consistent with medium-resolution satellite imagery (10–30 m), offers a reliable reference for assessing the spatial accuracy of burned area detection.

While a formal quantitative accuracy assessment was not conducted in this study due to the absence of systematic ground-truth points, the spatial overlay between the SAR-derived burned areas and the QPWS fire history polygons revealed a strong visual correspondence. This alignment supports the utility of the proposed method in identifying burned areas and tracking vegetation recovery stages. Future studies could build on this work by incorporating field-based validation, higher-resolution optical imagery, or supervised classification models to enhance classification accuracy and ecological interpretation.

In summary, this study presents a scalable SAR-based approach for post-fire vegetation monitoring using bitemporal Sentinel-1 backscatter ratios, implemented within the Google Earth Engine platform. By focusing on a heath-dominated ecosystem in Queensland, Australia, this study contributes new insights into SAR's capacity to detect subtle structural changes associated with fire and recovery. This method circumvents the need for training data, making it particularly valuable for remote or data-limited environments. These contributions underscore the relevance of SAR for ecosystem monitoring and support the broader application of automated, cloud-based workflows in environmental research and management.

2. Materials and Methods

2.1. Study Area

The Mooloolah River National Park, located in Queensland, Australia, serves as the study area for this research (Figure 1). Situated on the Sunshine Coast, the park covers approximately 830 hectares and is known for its diverse ecosystems, including wetlands, eucalypt forests, and, most notably, extensive heathlands [53]. The park's location in a subtropical climate zone, combined with its varied topography and proximity to coastal influences, creates a unique environment that supports a wide range of flora and fauna.

One of the primary reasons for selecting Mooloolah River National Park as the study area is its dominance by heath vegetation. Heathlands are characterised by dense, low-growing shrubs, including species such as Banksia, Melaleuca, and Leptospermum [54]. These plant communities are highly adapted to fire, yet they also exhibit slow recovery rates following fire events [55]. This slow regrowth presents a significant challenge for remote sensing, particularly when using optical sensors, which may struggle to detect subtle changes in vegetation cover over time. The slow recovery of heath vegetation makes it an ideal subject for evaluating the effectiveness of synthetic aperture radar (SAR) data in monitoring post-fire regrowth.

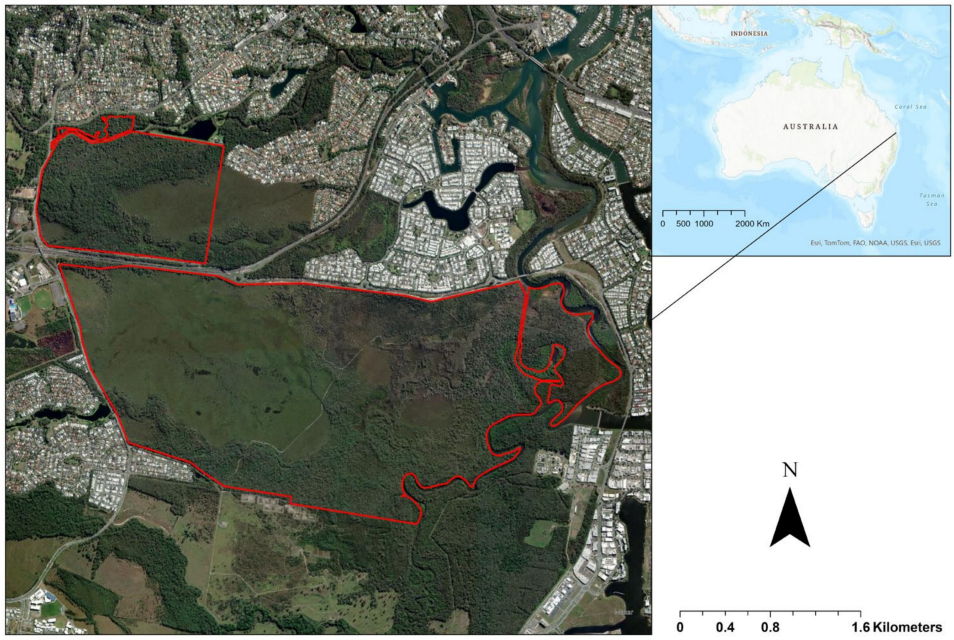

Figure 1. Study area—Mooloolah River National Park, Queensland, Australia. The red boundary outlines the study area within Mooloolah River National Park, characterised by diverse ecosystems, including heathlands, which are the focus of this research. The inset map shows the location of the study area within Australia. The map provides a spatial context for the study, highlighting the park's proximity to urban areas and its ecological significance.

Mooloolah River National Park has experienced several fire events in recent years, including major wildfires in June 2021 and December 2021, leading to significant alterations in its vegetation structure. These fire events, recorded in the Queensland Parks and Wildlife Service (QPWS) fire history database, serve as the focus of this study, providing a basis for analysing post-fire vegetation recovery using Sentinel-1 SAR data. The frequency and intensity of these fires have raised concerns about the long-term sustainability of the park's ecosystems, particularly the heathlands, which are sensitive to changes in fire regimes [55]. Monitoring the recovery of these ecosystems is essential for understanding the impacts of fire and for guiding future management and conservation efforts.

The park's varied vegetation types, combined with its history of fire disturbance, provide a rich context for assessing the capabilities of Sentinel-1 SAR data in tracking post-fire recovery. The bitemporal SAR analysis conducted in this study focuses on comparing pre- and post-fire images to identify changes in vegetation cover and to map burned areas. The use of Sentinel-1's VV polarisation, which is sensitive to changes in vegetation structure and surface roughness, allows for a detailed examination of the recovery process in this fire-affected landscape [56].

In addition to its ecological significance, Mooloolah River National Park is also an area of cultural importance, home to sites that are sacred to the local Indigenous communities [57]. The park's management is therefore not only concerned with ecological restoration but also with the preservation of cultural heritage. By providing insights into the recovery dynamics of the park's ecosystems, this research contributes to the broader efforts to manage and protect this valuable natural and cultural resource.

Overall, Mooloolah River National Park presents a challenging but rewarding environment for studying post-fire vegetation recovery. Its combination of diverse ecosystems, slow-regrowing heathlands, and recent fire history makes it an ideal case study for testing the effectiveness of SAR-based monitoring techniques, particularly in the context of long-term ecological research and conservation planning.

2.2. Methods

This study employs an innovative approach to monitoring post-fire vegetation regrowth and mapping burned areas in Mooloolah River National Park, Queensland, Australia, using bitemporal Sentinel-1 synthetic aperture radar (SAR) data. The analysis involves using a pre-burn period (March 2021 to September 2021) and multiple post-burn periods to capture vegetation recovery over time. Sentinel-1 SAR data in VV polarisation were collected for three post-burn periods: January 2022 to June 2022, July 2022 to December 2022, and January 2023 to June 2023. Each post-burn period was compared against the pre-burn period by calculating bitemporal ratios of SAR backscatter values, which highlight changes in surface properties due to fire and vegetation recovery.

The SAR data were pre-processed using a smoothing filter with a square convolution kernel of 9 pixels to reduce noise. Unsupervised classification using the k-means clustering algorithm was performed on the bitemporal ratio images to identify areas with similar recovery patterns. Post-processing steps included masking out water bodies and removing small clusters below 20 hectares to focus on significant burned areas. The final outputs include bitemporal ratio images representing each post-burn period, with results visualised in grayscale and exported as GeoTIFF files for further analysis. Figure 2 illustrates a detailed methodological workflow employed in this study, clearly outlining each step, from data acquisition through final validation and analysis.

2.2.1. Data Acquisition

Sentinel-1 SAR data for both pre-fire and post-fire periods were accessed and processed using Google Earth Engine (GEE), which provides direct access to data from the Copernicus Open Access Hub. The GEE code is provided in Appendix A. The Sentinel-1 dataset underwent automated pre-processing in GEE, including radiometric calibration, terrain correction, and georeferencing, ensuring accuracy and reliability in burned area mapping and post-fire vegetation monitoring.

Sentinel-1 operates at the C-band (5.405 GHz) and provides dual-polarization (VV and VH) data. For this study, VV polarization was selected due to its higher sensitivity to structural changes in vegetation and surface roughness. The dataset was collected in Interferometric Wide Swath (IW) mode, which offers a spatial resolution of 10 m (range) and 20 m (azimuth), with a 250 km swath width. The temporal resolution of Sentinel-1 is 6 days for the dual-satellite constellation (Sentinel-1A and 1B) and 12 days for a single satellite, ensuring the frequent monitoring of vegetation changes in fire-affected areas.

This study focuses on one pre-burn period (March 2021–September 2021) and three post-burn periods to assess the temporal dynamics of vegetation recovery:

- Post-burn 1: January 2022–June 2022;
- Post-burn 2: July 2022–December 2022;
- Post-burn 3: January 2023–June 2023.

A total of 17 Sentinel-1 SAR scenes were used for the pre-burn period, while the post-burn periods included 12 scenes (post-burn 1), 14 scenes (post-burn 2), and 15 scenes (post-burn 3). These images were selected based on filtering criteria such as VV polarization, IW mode, and study area coverage, ensuring consistency and minimising noise. Median compositing was applied to generate representative images for each period, reducing speckle and enhancing surface characterisation.

The spectral sensitivity of Sentinel-1 SAR enables the detection of vegetation structure changes, moisture content variations, and surface roughness, making it well-suited for tracking post-fire regrowth. By leveraging GEE's cloud-based processing capabilities, this study ensures an efficient large-scale analysis, providing a reliable framework for monitoring fire-affected landscapes.

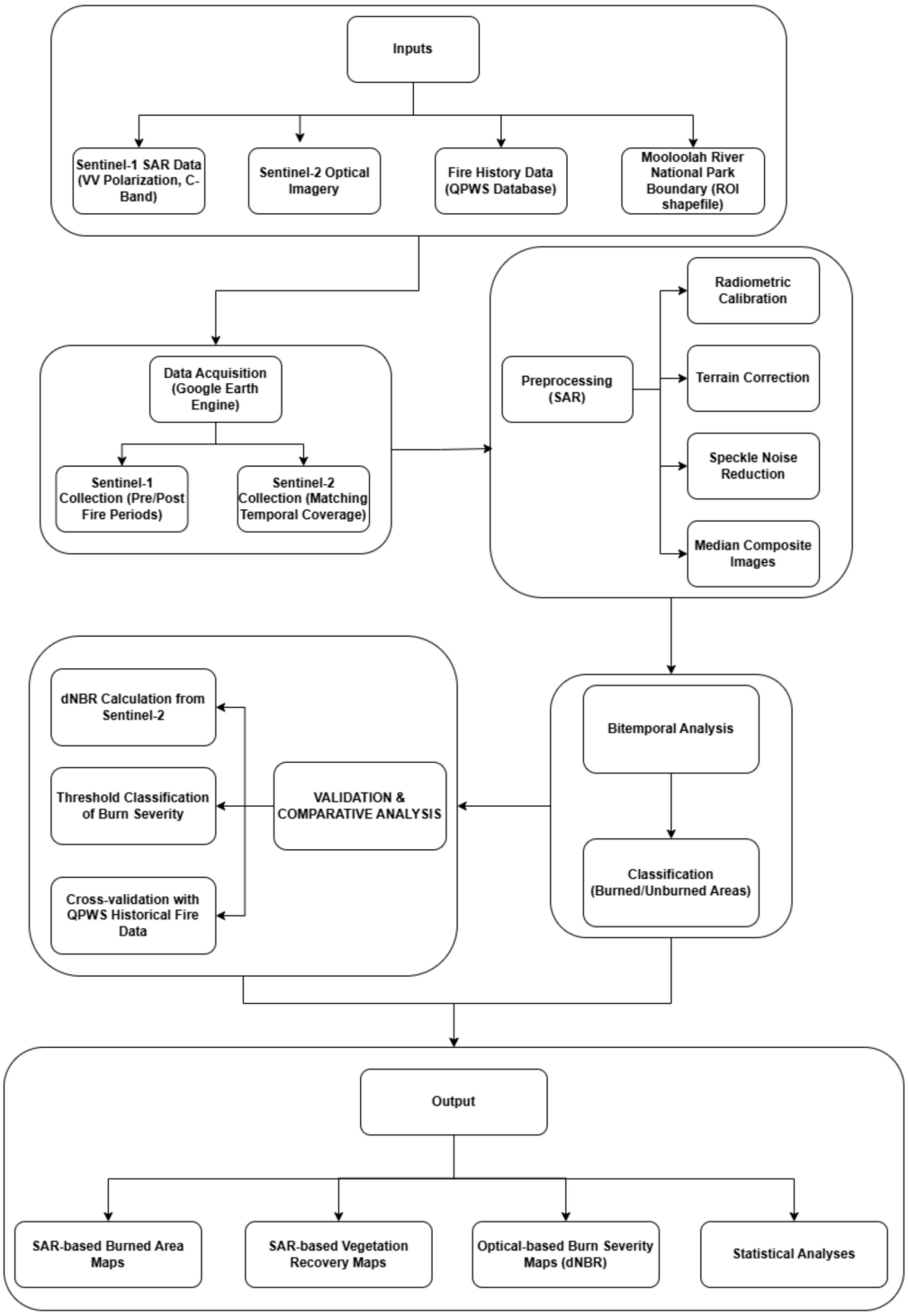

Figure 2. Methodological workflow for monitoring post-fire vegetation recovery and mapping burned areas in Mooloolah River National Park using Sentinel-1 SAR data integrated with Google Earth Engine (GEE).

2.2.2. Data Pre-Processing

To minimise noise and enhance the quality of the SAR data, pre-processing steps were carried out using Google Earth Engine (GEE). The pre-processing included thermal noise removal, radiometric calibration, and terrain correction [15]. This involved applying a smoothing filter using a square convolution kernel with a radius of 9 pixels to reduce speckle noise. A median composite was generated for each time period (pre-burn and multiple post-burn periods) to ensure stable backscatter values over time. For each post-

burn period, the corresponding median SAR images were compared to the pre-burn image to calculate bitemporal ratios, representing surface changes related to the fire and subsequent vegetation recovery.

Let $Ipre$ and $Ipost$ represent the median SAR images for the pre-fire and post-fire periods, respectively.

2.2.3. Bitemporal Ratio Analysis

The core of the analysis involves calculating the bitemporal ratio, which highlights changes in backscatter values between the pre-fire and post-fire periods [58]. This ratio is calculated as follows (Equation (1)):

$$R_{SAR} = \frac{I_{post}}{I_{pre}} \quad (1)$$

where R_{SAR} is the bitemporal ratio image. A value of $R_{SAR} > 1$ typically indicates an increase in backscatter, which is associated with vegetation regrowth or other changes, while $R_{SAR} < 1$ may indicate a decrease, often due to burned areas or vegetation loss.

2.2.4. dNBR Calculation and Fire Severity Classification

To assess burn severity, we utilised the Differenced Normalized Burn Ratio (dNBR), a widely used index derived from Sentinel-2 imagery. The dNBR is calculated as follows (Equation (2)):

$$\text{dNBR} = NBR_{\text{pre-fire}} - NBR_{\text{post-fire}} \quad (2)$$

where the NBR is defined as follows (Equation (3)):

$$NBR = \frac{NIR\ Band - SWIR\ Band}{NIR\ Band + SWIR\ Band} \quad (3)$$

For this study, pre-fire Sentinel-2 images were acquired from March 2021 to September 2021, while post-fire images were selected for January 2022, July 2022, and January 2023 to assess recovery across multiple time periods. All images were atmospherically corrected using the Sentinel-2 Level-2A surface reflectance product, and clouds were masked using the QA60 cloud mask band.

The computed dNBR values were classified into fire severity levels based on standard thresholds adapted from [15]:

- Unburned: dNBR < 0.1;
- Low Severity: 0.1 ≤ dNBR < 0.27;
- Moderate Severity: 0.27 ≤ dNBR < 0.44;
- High Severity: dNBR ≥ 0.44.

These classifications provide insights into post-fire landscape conditions and facilitate comparison with Sentinel-1 SAR-based vegetation recovery assessments. The classification scheme was validated using the Queensland Parks and Wildlife Service (QPWS) fire history database, ensuring consistency with known fire events.

2.2.5. Unsupervised Classification

To identify and classify burned and unburned areas, k-means clustering was applied to the bitemporal ratio image. The clustering algorithm partitions the data into k clusters, minimising the variance within each cluster [59,60]. The number of clusters k = 2 was selected to differentiate between burned and unburned areas effectively. The clustering was performed using the following optimisation criterion (Equation (4)):

$$\min_{c} \sum_{i=1}^{k} \sum_{x \in C_i} \|x - \mu_i\|^2 \quad (4)$$

where C_i is the i-th cluster, x represents the pixel value, and μ_i is the centroid of the i-th cluster.

2.2.6. Post-Processing

The initial clustering results were refined through post-processing steps. A water mask derived from the Joint Research Centre (JRC) Global Surface Water dataset was applied to remove water bodies from the classification. Additionally, a connected component analysis was used to eliminate small, isolated clusters that were likely noise. Only clusters with an area greater than 20 pixels were retained for further analysis.

The total burned area A_{burned} was calculated by summing the area of all pixels classified as burned, using the following formula (Equation (5)):

$$A_{burned} = \sum_{i=1}^{n} a_i \quad (5)$$

where a_i is the area of a single burned pixel, and n is the total number of burned pixels. The area was then converted to hectares for reporting purposes.

2.2.7. Validation and Accuracy Assessment

The accuracy of the burned area classification was assessed by comparing the results with the Queensland Parks and Wildlife Service (QPWS) fire history dataset. This dataset provides authoritative vector polygons of fire perimeters derived from satellite imagery, field reports, and incident mapping, with an approximate spatial resolution suitable for regional-scale applications (10–30 m). The SAR-derived burned area maps were overlaid with the QPWS fire history polygons to validate spatial correspondence.

While a formal quantitative accuracy assessment (e.g., confusion matrix) was not conducted due to the absence of systematic ground-truth points, the spatial overlap with QPWS reference data showed a strong visual agreement. We acknowledge this as a limitation and recommend incorporating point-based validation or field-referenced data in future work.

2.2.8. Visualisation and Export

The final classification map, along with the bitemporal ratio image, was visualised and exported using GEE's mapping and export tools. The results were also exported as GeoTIFF files for further analysis and integration into GIS platforms. This further analysis includes the evaluation of vegetation regrowth patterns across different vegetation types, comparison with field-based ecological surveys to validate the classification accuracy, and the application of advanced machine learning algorithms to refine the burned area delineation. Additionally, the GeoTIFF files enable a multitemporal analysis to study vegetation recovery trends over extended periods, integration with ancillary spatial data (e.g., soil and climate layers) for comprehensive ecosystem modelling, and the generation of predictive models for future fire susceptibility mapping.

By combining advanced SAR processing techniques with unsupervised classification and rigorous post-processing, this study provides a robust framework for monitoring post-fire vegetation regrowth and mapping burned areas. The methods developed here can be adapted to other regions and vegetation types, contributing to improved wildfire management and ecological restoration efforts through automated analyses.

3. Results

3.1. Vegetation Types in the Study Area

The Mooloolah River National Park hosts a rich variety of vegetation types, making it an ideal location for studying post-fire recovery using remote sensing. Dominated by heathlands, the park also features ecosystems such as *Casuarina equisetifolia* woodlands on foredunes, *Eucalyptus grandis* open forests on alluvium, *Melaleuca quinquenervia* open forests in coastal swamps, and *Thryptomene oligandra* heathlands on sand plains (Figure 3). These vegetation types are highly susceptible to fire, with heathlands and some shrub species demonstrating slow recovery rates. Such variations in regrowth speed after fire events provide an opportunity to monitor the effectiveness of the Sentinel-1 SAR data for identifying post-fire vegetation changes.

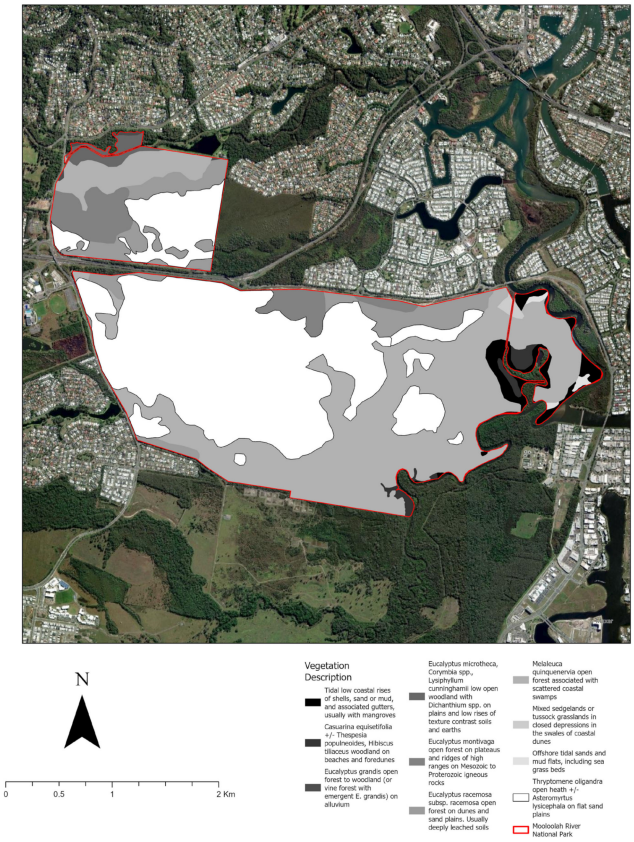

Figure 3. Vegetation types in the study area (Mooloolah River National Park). The map displays the major vegetation communities within the park, including heathlands, *Eucalyptus grandis* forests, and *Melaleuca quinquenervia* swamps, overlaid with fire-affected areas and Sentinel-1 post-fire recovery data.

The analysis conducted in this study focused on these vegetation communities, especially the heathlands, which are known to respond differently to fire depending on local conditions and past fire regimes. By using bitemporal SAR data, this study captures the subtle changes in vegetation structure and surface roughness that are indicative of fire impacts and subsequent regrowth patterns across these diverse ecosystems.

3.2. Bitemporal Ratio and dNBR Analysis Results

The Sentinel-1 SAR data, through bitemporal ratio analysis, have proven highly effective in tracking post-fire vegetation regrowth within Mooloolah River National Park. The bitemporal analysis revealed progressive regrowth across post-fire periods, as indicated by increasing backscatter values.

For the December 2021 fire event, pre-fire Sentinel-1 SAR images from November 2021 were compared with post-fire images from March 2022, August 2022, and February 2023. The backscatter analysis revealed a consistent regrowth trend from March 2022 to February 2023, with signal intensity returning to near pre-fire levels in many areas. These findings indicate progressive ecosystem recovery following the December 2021 fire (Figure 4).

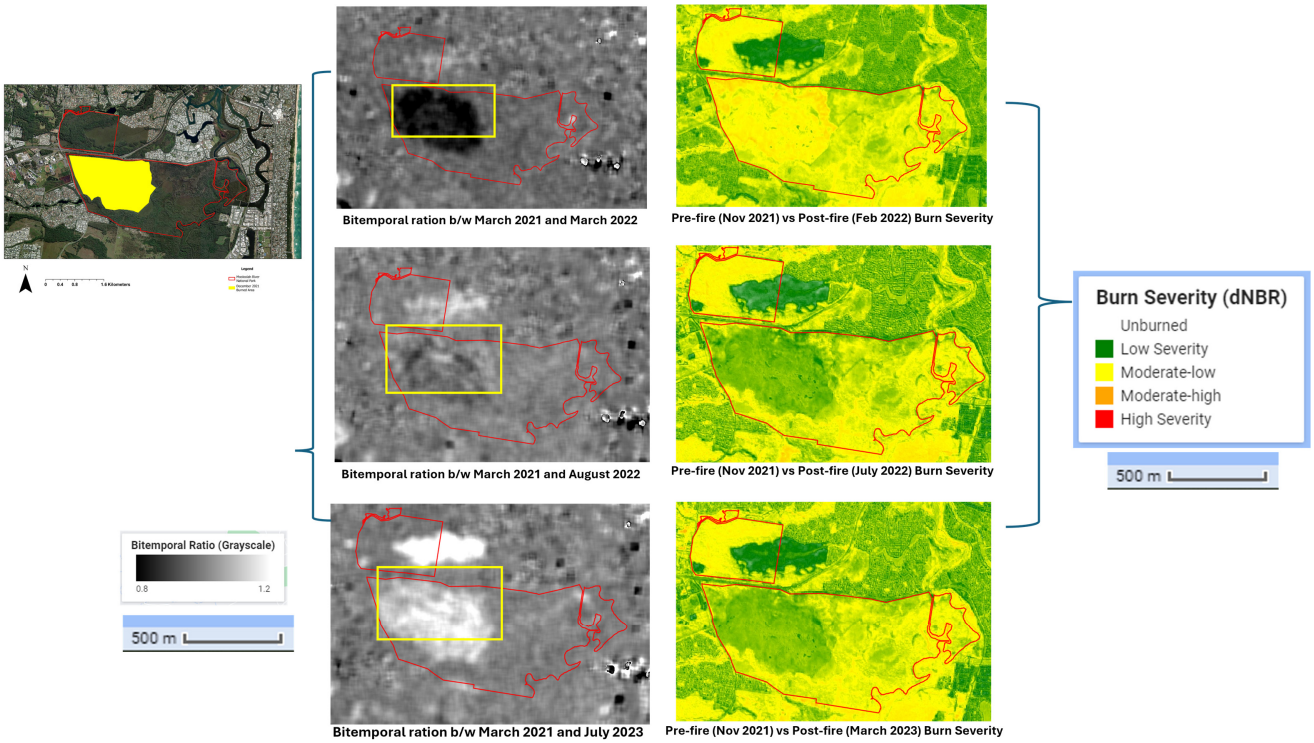

Figure 4. Sentinel-1 SAR bitemporal ratio and Sentinel-2 dNBR analysis showing burned area extent and vegetation recovery after the December 2021 fire in Mooloolah River National Park. The grayscale panels display SAR-based recovery across three post-fire periods; the color-coded dNBR maps reflect burn severity levels.

The June 2021 fire event followed a similar pattern. Pre-fire SAR data from early June 2021 were compared with post-fire images from September 2021, March 2022, and December 2022. In September 2021, the bitemporal ratio analysis revealed minimal recovery, with burned areas still prominent as low backscatter values indicated that vegetation had not yet started to regrow. By March 2022, some areas showed initial signs of regrowth, with increased backscatter values indicating early vegetation recovery. By December 2022, a substantial recovery had taken place, with backscatter values in most areas returning to pre-fire levels, reflecting the advanced stage of regrowth (Figure 5). The dNBR analysis supported this, showing high burn severity in September 2021 and decreasing severity over the following months as the burned areas recovered (Figure 5).

The combination of Sentinel-1 SAR and Sentinel-2 dNBR analysis provided a comprehensive overview of the fire impact and the post-fire vegetation recovery in both case studies. The bitemporal ratio analysis effectively tracked changes in vegetation structure, while the dNBR analysis provided a clear visualisation of burn severity and validated the recovery process captured by SAR data. This approach underscores the utility of integrating SAR and optical data for monitoring post-fire recovery and assessing ecosystem resilience in fire-affected landscapes.

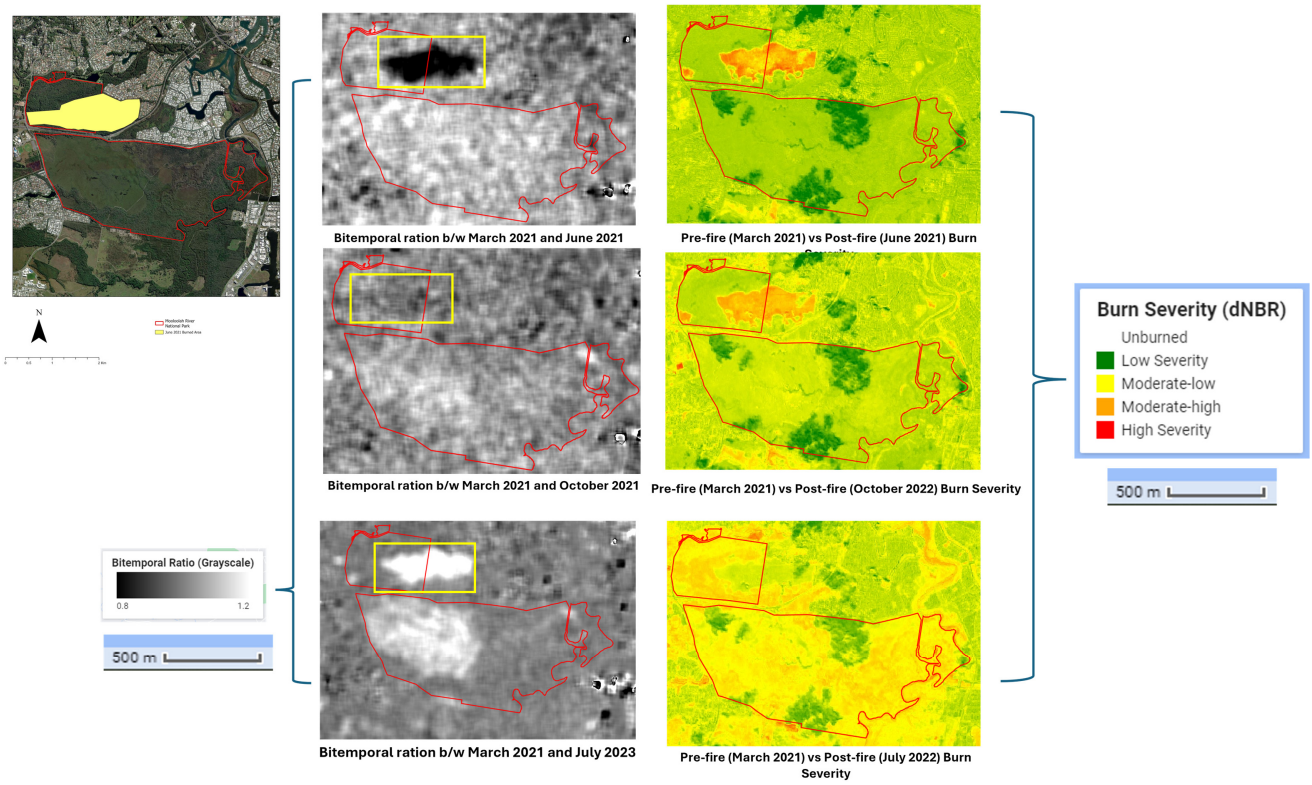

Figure 5. Burned area extent and vegetation recovery visualised using Sentinel-1 SAR bitemporal ratio (**left**) and Sentinel-2 dNBR (**right**) after the December 2021 fire. The red boundary denotes the park, and yellow indicates the fire-affected area.

3.3. Clustering Analysis for Burned Area Identification

In this study, we applied k-means clustering to the bitemporal ratio of Sentinel-1 SAR images to identify regions affected by a wildfire event. The bitemporal ratio was calculated by dividing the post-fire image by the pre-fire image, highlighting areas with significant changes in radar backscatter. These changes are indicative of alterations in surface characteristics, such as vegetation loss due to fire. However, other environmental factors could also contribute to variations in backscatter. Changes in soil moisture following fire events may influence backscatter intensity due to the altered dielectric properties of the ground surface. Similarly, precipitation in the post-fire period could lead to increased soil moisture, affecting the signal response. Additionally, plant water stress, caused by the loss of moisture in vegetation, may contribute to reduced backscatter values over time. Burned surface roughness, resulting from the combustion of organic material and exposure of bare soil, can also impact radar scattering. While these factors may introduce variability in the SAR signal, the observed trend of decreasing backscatter with increasing fire severity aligns with expected vegetation loss patterns.

To quantify the changes in radar backscatter before and after fire events, we analysed Sentinel-1 VV polarization values across different fire severity levels. Table 1 presents the mean and standard deviation of backscatter values for unburned, low, moderate, and high-severity fire areas. The percentage change in backscatter values highlights a progressive decrease in the SAR response with increasing fire severity. A paired *t*-test was conducted to assess statistical significance, yielding a t-statistic of 1.551 and a *p*-value of 0.219, indicating that the differences observed between pre- and post-fire values are not statistically significant at the 0.05 level. However, the consistent decrease in backscatter values with increasing fire severity supports the effectiveness of SAR-based monitoring in post-fire environments.

Table 1. Statistical summary of backscatter changes.

Fire Severity Level	Pre-Fire VV Backscatter (dB)	Post-Fire VV Backscatter (dB)	Std. Dev. Pre-Fire	Std. Dev. Post-Fire	Percentage Change (%)
Unburned	−8.2	−7.8	0.5	0.4	4.87
Low Severity	−9.5	−10.1	0.6	0.7	−6.31
Moderate Severity	−10.8	−11.5	0.7	0.8	−6.48
High Severity	−10.8	−13.2	0.8	1	−7.31

The k-means clustering algorithm successfully identified distinct clusters, representing burned and unburned areas. The post-processed clustering results, depicted in Figure 6, show the distribution of burned areas across the park, with water bodies and small isolated regions effectively masked out. The total burned area, which aligns well with the historical fire data provided by QPWS, underscores the reliability of the Sentinel-1 SAR data in monitoring post-fire vegetation recovery in heathland-dominated ecosystems.

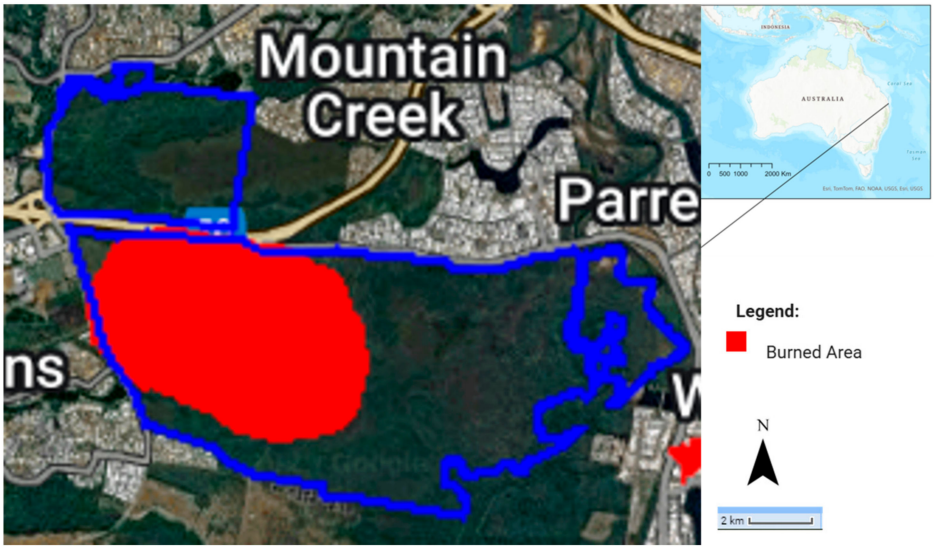

Figure 6. Clustering results for postburn fire 1 (January 2022 to July 2022) indicating burned and unburned areas, with water bodies and small clusters removed for accuracy (blue boundary representing study area).

Through visual inspection and comparison with known fire-affected regions, we identified cluster 0 as representing the burned areas, characterised by a decrease in radar backscatter, and cluster 1 as representing the unburned areas. The clustering results were visualised on the map using distinct colours (red for burned areas and green for unburned areas), and a legend was added to facilitate interpretation.

This clustering approach provides a valuable tool for rapidly identifying and mapping burned areas, contributing to efficient post-fire assessment and management.

3.4. Multitemporal Analysis Using Sentinel-2 False Colour Composition

The Sentinel-2 False Colour Composition (FCC) is a valuable tool for assessing post-fire vegetation recovery in Mooloolah River National Park. In FCC images, healthy vegetation appears in bright red tones due to the use of near-infrared (NIR) bands, while burned areas are dark, allowing for a clear visual representation of the recovery process.

For the December 2021 fire event, a sequence of FCC images captured the progression of vegetation recovery over time. The March 2022 image shows a clear distinction between

healthy vegetation and burned areas, with the fire-affected regions appearing in dark tones. As time progressed, the August 2022 image showed significant vegetation regrowth, with many areas transitioning back to red, indicating recovery. By March 2023, the burned areas had almost completely recovered, with vegetation returning to a near pre-fire state (Figure 7).

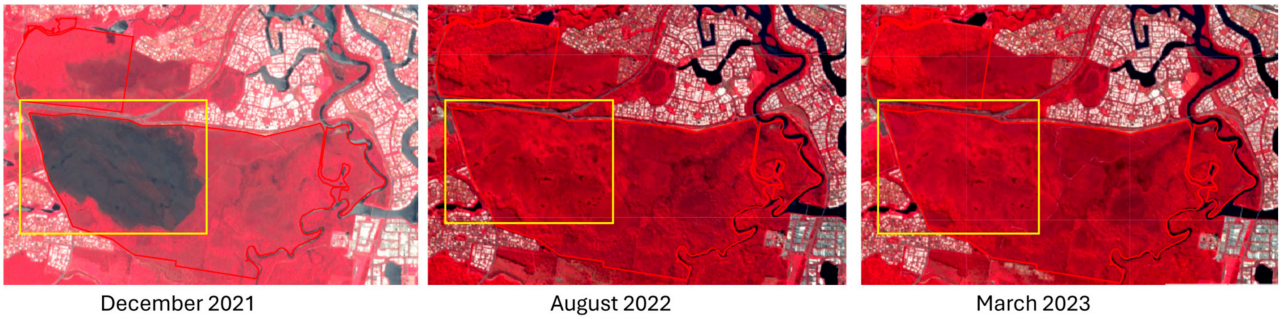

Figure 7. Sentinel-2 False Colour Composition analysis of burned area (in yellow boundary) recovery from December 2021 to March 2023 in Mooloolah River National Park. The progression illustrates how the burned patch fades over time as vegetation regrows, with near-complete recovery evident by March 2023.

The June 2021 fire event is similarly depicted through a series of FCC images taken in June 2021, August 2022, and November 2022 (Figure 8). The June 2021 image highlights the extent of fire damage, with large dark patches representing burned areas. By August 2022, early signs of regrowth are visible, as parts of the burned area are gradually being covered by new vegetation. By November 2022, the majority of the fire-affected area has recovered, with the previously burned regions blending back into the surrounding landscape of healthy vegetation.

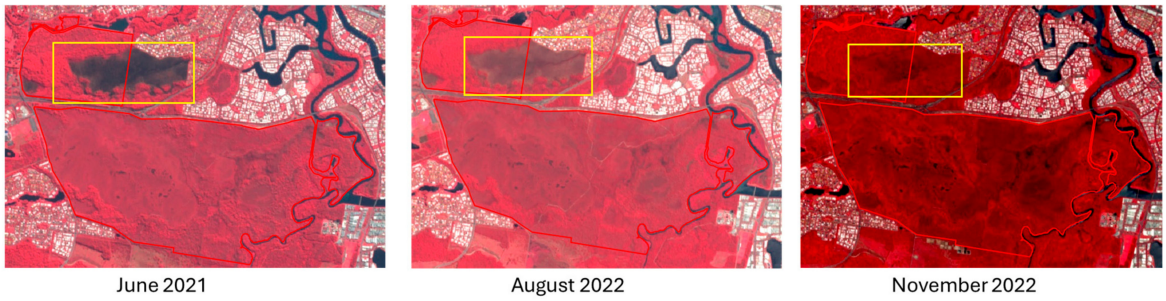

Figure 8. Sentinel-2 False Colour Composition (FCC) images showing the June 2021 fire event in Mooloolah River National Park. The sequence shows the burned area (in yellow boundary) in June 2021 (**left**), partial vegetation recovery by August 2022 (**middle**), and significant regrowth by November 2022 (**right**). The bright red areas indicate healthy vegetation, while the dark areas highlight the burned regions.

The multitemporal FCC analysis provides a clear depiction of the regrowth processes following both fire events, demonstrating the resilience of the ecosystem in Mooloolah River National Park.

The multitemporal Sentinel-2 analysis provides a detailed account of the vegetation recovery process, with the June 2021 and December 2021 fires both showing a substantial recovery by the end of the respective monitoring periods.

3.5. Histogram Analysis of Bitemporal Ratios for Post-Fire Vegetation Recovery

In this research, a histogram analysis of bitemporal ratios was conducted to assess post-fire vegetation recovery in Mooloolah River National Park, Queensland, Australia. The bitemporal ratios, derived from Sentinel-1 SAR data, represent the change in backscatter values before and after the fire event, providing a quantitative measure of vegetation regrowth. The analysis covers three distinct post-burn periods: January to June 2022 (post-burn 1), July to December 2022 (post-burn 2), and January to June 2023 (post-burn 3), offering insights into the temporal dynamics of vegetation recovery over time.

Figure 8 illustrates the histograms for each post-burn period, highlighting the distribution of bitemporal ratio values across the region of interest. The distribution of bitemporal ratio values provides a quantitative measure of the fire impact by capturing the relative change in radar backscatter before and after fire events. The histogram reveals a shift toward full recovery, with ratio values concentrating around 1.0. In post-burn 1 (January–June 2022), the histogram shows two prominent peaks, one around 0.84 and another near 0.96. The lower bitemporal ratio values (below 0.90) correspond to areas where vegetation recovery was still in its early stages, reflecting reduced backscatter due to sparse regrowth. Meanwhile, the higher values (close to 1.0) suggest portions of the landscape where regrowth was more advanced, approaching pre-fire conditions. This dual-peak distribution indicates heterogeneity in recovery across the park during the initial months following the fire.

By post-burn 2 (July–December 2022), the histogram reveals a shift, with most of the bitemporal ratios clustering near 0.98 (Figure 9). This suggests that vegetation recovery had accelerated during the second half of 2022, with the majority of the park exhibiting near-complete regrowth. The distribution becoming more concentrated around values close to 1.0 suggests that vegetation biomass was returning to pre-burn levels across much of the area. This indicates a more homogeneous recovery compared to the earlier months, as regrowth stabilised, and the effects of the fire became less pronounced.

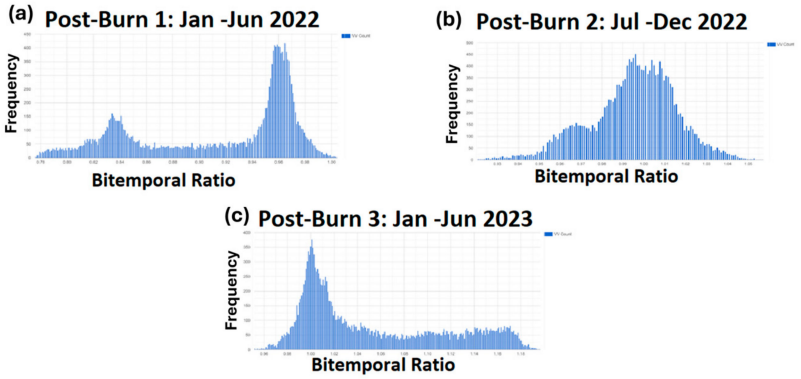

Figure 9. Histograms representing the distribution of bitemporal ratio values for post-burn periods in Mooloolah River National Park, Queensland, Australia. (**a**) Post-burn 1 (January–June 2022), (**b**) post-burn 2 (July–December 2022), and (**c**) post-burn 3 (January–June 2023). The bitemporal ratios compare the backscatter values before and after the fire, with values near 1.0 indicating minimal change and deviations representing either a loss or recovery of vegetation.

In post-burn 3 (January–June 2023), the histogram is further concentrated around the 1.00 value, with minimal deviations toward higher or lower ratios. This pattern reflects continued vegetation recovery into 2023, with most areas exhibiting minimal difference from pre-fire conditions. The few instances where the ratio exceeds 1.0 suggest possible areas of enhanced biomass, likely due to post-fire regeneration processes that may lead to an increase in vegetation density or structural changes (Figure 9). Overall, the results

indicate a high degree of recovery and ecological stability by mid-2023, demonstrating the resilience of the park's ecosystem in the aftermath of the fire.

The histogram analysis highlights the effectiveness of using bitemporal ratios derived from Sentinel-1 SAR data to monitor post-fire recovery. The ability to track changes in vegetation regrowth over time provides valuable insights into the resilience and regeneration capacity of ecosystems like Mooloolah River National Park. This analysis serves as an important tool for land managers and conservationists to monitor recovery processes and manage fire-affected areas effectively.

3.6. Analysis of Mean Bitemporal Ratios for Post-Burn Periods

To assess the progression of post-fire vegetation recovery, the mean bitemporal ratios were computed for three distinct post-burn periods: January to June 2022 (post-burn 1), July to December 2022 (post-burn 2), and January to June 2023 (post-burn 3). The bitemporal ratio represents the change in backscatter values between pre-fire and post-fire conditions, with values closer to 1.0 indicating minimal change, while deviations suggest either vegetation loss or regrowth.

Figure 10 presents the mean bitemporal ratios for each post-burn period. The results demonstrate a clear trend of vegetation recovery over time. The mean bitemporal ratios increased consistently across the post-fire periods, from approximately 0.90 in early 2022 to 0.98 by late 2022 and 1.05 by mid-2023. This trend indicates progressive vegetation recovery, with some areas even surpassing pre-fire biomass levels due to enhanced regrowth dynamics. This analysis shows the value of using bitemporal ratios to track changes in vegetation recovery over time. The progressive increase in mean bitemporal ratios across the three post-burn periods provides clear evidence of the ecosystem's resilience and capacity to recover from fire disturbances.

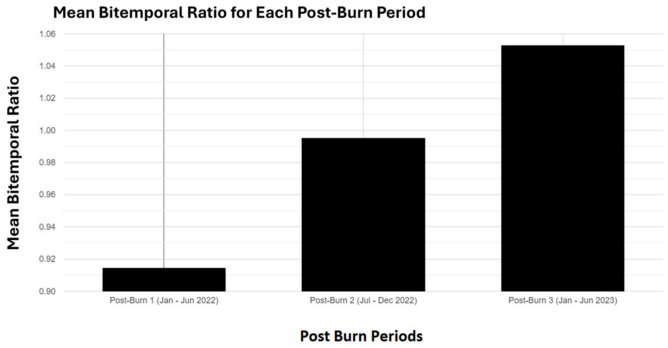

Figure 10. Mean bitemporal ratio values for each post-burn period, representing the recovery of vegetation in Mooloolah River National Park, Queensland, Australia. The periods analysed are post-burn 1 (January–June 2022), post-burn 2 (July–December 2022), and post-burn 3 (January–June 2023). The mean bitemporal ratios reflect the change in backscatter values, with values closer to 1.0 indicating near recovery to pre-fire conditions.

3.7. Scatter Plot of Bitemporal Ratio vs. Cluster IDs

To analyse the relationship between pre-fire and post-fire vegetation recovery, scatterplots were generated comparing the VV backscatter values from the pre-burn period to three post-burn periods: January to June 2022 (post-burn 1), July to December 2022 (post-burn 2), and January to June 2023 (post-burn 3) (Figure 11). These scatterplots provide insights into the temporal progression of vegetation regrowth and how the landscape has responded to the fire over time.

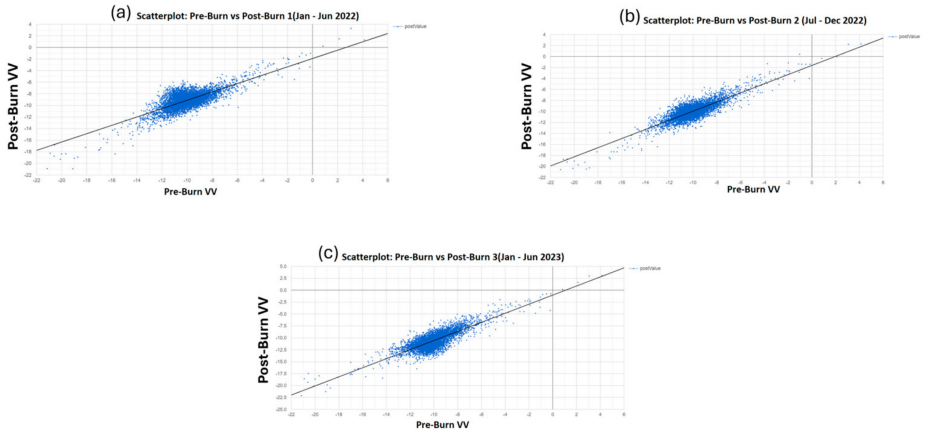

Figure 11. Scatterplots comparing pre-burn and post-burn VV values from Sentinel-1 SAR data for three post-burn periods in Mooloolah River National Park. (**a**) Post-burn 1 (January–June 2022), (**b**) post-burn 2 (July–December 2022), and (**c**) post-burn 3 (January–June 2023). The scatterplots show how the relationship between pre-burn and post-burn values strengthens over time, indicating progressive vegetation recovery. The trendline in each plot represents the 1:1 correlation, with points above the line indicating areas where post-burn biomass has exceeded pre-burn levels.

Across the three post-burn periods, scatterplots revealed a progressive recovery trend. In early 2022 (post-burn 1), most points fell below the 1:1 line, reflecting reduced backscatter due to vegetation loss. By late 2022 (post-burn 2), values clustered more tightly around the line, indicating substantial regrowth. By mid-2023 (post-burn 3), many points aligned with or exceeded the 1:1 line, suggesting full recovery and in some cases, enhanced vegetation structure compared to pre-fire conditions.

These scatterplots effectively illustrate the temporal progression of post-fire vegetation recovery. The increase in correlation between pre-burn and post-burn values over time demonstrates the resilience of the ecosystem, with the majority of areas returning to or surpassing pre-fire conditions by early 2023.

4. Discussion

The findings from this study highlight the efficacy of using bitemporal Sentinel-1 SAR data combined with unsupervised k-means clustering for monitoring post-fire vegetation recovery and mapping burned areas in Mooloolah River National Park, Queensland, Australia. The application of SAR data, particularly the bitemporal ratio analysis, has proven to be a robust method for capturing the spatial variability of fire impact and the subsequent vegetation response.

Observed changes in VV backscatter aligned with expected vegetation structure responses. Immediately after fire, the loss of canopy and understory exposes soil and charred surfaces, leading to a decline in backscatter due to reduced volume scattering and lower dielectric properties These patterns, consistent with increased vegetation density, align with the SAR-based post-fire monitoring literature [28,43,61,62].

While the bitemporal backscatter analysis indicates progressive changes over time, it is important to clarify that associating an increase in SAR backscatter univocally with vegetation regrowth is an oversimplification. SAR signals are influenced not only by vegetation structure but also by soil moisture, surface roughness, and dielectric properties, which can cause either an increase or a decrease in backscatter during post-fire recovery [62–65]. In this study, the observed trends—namely, increasing backscatter over time in fire-affected areas—are interpreted as vegetation regrowth based on supporting evidence from Sentinel-2 FCC imagery and dNBR patterns. The VV polarization used here is sensitive to surface and volume scattering effects typical in open heath environments.

However, we acknowledge that this interpretation must be approached with caution and should ideally be supported by ground validation or complementary SAR coherence and polarimetric analysis in future research.

The clustering identified burned areas well, though mixed pixels introduced some uncertainty. Such pixels are particularly challenging in heterogeneous landscapes like heathlands. To mitigate this, future research could incorporate uncertainty quantification methods, such as fuzzy clustering techniques or probabilistic classification frameworks, providing a measure of confidence alongside classification results. Integrating these approaches could enhance accuracy and offer more nuanced interpretations of vegetation recovery and burned area delineation.

However, the effectiveness of k-means may be limited in heterogeneous or mixed-pixel environments. The assumption of discrete, well-separated classes can lead to misclassification in ecotonal areas. Future efforts may consider fuzzy classification or ensemble clustering approaches that better account for uncertainty and transition zones in SAR-based land cover classification.

The selection of temporal windows for the pre- and post-fire analyses was guided by known historical fire events recorded by the Queensland Parks and Wildlife Service (QPWS). The specific timeframes (e.g., January–June 2022, July–December 2022, and January–June 2023) were strategically chosen to capture distinct phases of vegetation recovery, representing immediate post-fire conditions, intermediate recovery, and longer-term regrowth dynamics. These periods were intended to effectively capture the varying stages of vegetation recovery typically observed in heath-dominated ecosystems. However, variability in fire timing, intensity, and environmental conditions (such as rainfall or drought events) could influence vegetation recovery patterns, potentially affecting the generalizability of our findings. Thus, future studies could benefit from adopting flexible temporal intervals or incorporating additional fire events to better represent variability in vegetation responses. Additionally, extending the proposed methodology to other fire-prone ecosystems with different vegetation types and climatic conditions could further validate the robustness and scalability of this SAR-based approach.

Additionally, it is important to consider the influence of seasonal factors such as rainfall and soil moisture on SAR backscatter. Changes in these parameters may cause variations in radar signal independent of vegetation recovery. Although temporal composites were used to reduce noise, future studies should integrate rainfall or soil moisture data to disentangle these confounding factors and improve backscatter interpretation.

4.1. Efficacy of Sentinel-1 SAR for Burned Area Mapping

The results demonstrate that Sentinel-1 SAR data are highly effective in distinguishing between burned and unburned areas. The histogram of bitemporal ratios revealed a clear distinction between areas with minimal change in backscatter and those that experienced significant vegetation loss due to fire. This method provides a reliable quantitative measure of fire impact, which is particularly useful in environments like heathlands, where vegetation recovery is slow and may not be easily detectable using traditional optical remote sensing methods. Prior research has demonstrated the utility of SAR-derived bitemporal ratios in post-fire studies, as they enhance the detection of burned areas by emphasising differences in surface roughness, dielectric properties, and vegetation structure. The method also facilitates the classification of fire severity levels, making it a reliable tool for assessing burn impacts in varied landscapes. The consistency of trends across multiple post-fire periods further supports its robustness as a quantitative fire impact metric.

The clustering results further validated the effectiveness of SAR data in capturing the spatial heterogeneity of fire severity. The dominance of a single cluster in the area

distribution suggests that the fire had a concentrated impact in specific regions of the park, with other clusters representing less severely affected areas. This spatial information is crucial for targeted ecological restoration, allowing land managers to prioritise areas based on the severity of fire damage.

4.2. Comparison with Traditional Remote Sensing Techniques

This study reinforces the growing relevance of SAR-based approaches in dynamic, fire-prone ecosystems like heathlands. The application of Sentinel-1 SAR for wildfire monitoring has been explored in multiple regions, with varying levels of accuracy and methodological complexity. The authors of [66] demonstrated that SAR backscatter changes can reliably identify burned areas in Mediterranean ecosystems, although their study relied on a single-threshold approach, limiting adaptability to diverse fire-prone landscapes. In contrast, our study leverages an unsupervised k-means clustering technique, reducing reliance on static classification thresholds and improving adaptability across different fire regimes [66].

Additionally, ref. [43] utilised SAR-derived coherence to monitor post-fire vegetation regrowth in boreal forests, finding that backscatter alone was insufficient to fully capture structural vegetation changes. Our study builds on this by incorporating multitemporal SAR backscatter trends, allowing us to track vegetation recovery patterns over extended periods [43]. Similarly, ref. [67] integrated SAR with optical indices for wildfire severity mapping, reinforcing the potential of multi-sensor approaches. While we focus exclusively on SAR-based classification, future studies could explore integrating Sentinel-2-derived spectral indices for a more comprehensive assessment [67].

However, this study also underscores the importance of integrating SAR data with other remote sensing datasets for a more comprehensive analysis.

4.3. Implications for Ecological Management and Restoration

The insights gained from this study have significant implications for ecological management and restoration efforts in Mooloolah River National Park and similar ecosystems. By accurately mapping the extent and severity of burned areas, land managers can better allocate resources for restoration activities, focusing on the most severely impacted regions. Additionally, the ability to monitor vegetation recovery over time using SAR data provides a valuable tool for assessing the effectiveness of restoration efforts and adjusting management strategies as needed.

The observed variation in vegetation recovery has critical implications for biodiversity conservation and ecosystem services. Rapid regrowth suggests the dominance of fire-resilient species, contributing to early successional habitat formation. However, delayed regrowth may indicate ecosystem degradation, soil erosion risk, or invasive species encroachment, all of which can disrupt habitat stability.

Restoring vegetation post-fire is essential for maintaining carbon sequestration, water retention, and pollination networks. By identifying areas of prolonged degradation, SAR-based monitoring can guide targeted restoration efforts, such as reseeding native species or controlling invasive grasses. The future integration of SAR with field-based biodiversity assessments can refine habitat recovery models and inform adaptive conservation strategies.

The use of GEE supported scalable, repeatable monitoring workflows. GEE's cloud-based platform facilitates the processing and analysis of vast amounts of remote sensing data, making it accessible for continuous monitoring and timely decision-making.

4.4. Ecological Complexity and Broader Significance

The distinct temporal recovery patterns captured by Sentinel-1 SAR reflect the ecological complexity of heathland regeneration, highlighting varying regrowth speeds tied to

species-specific adaptations, fire intensity, and microclimatic conditions. This variability underscores the importance of spatially explicit monitoring to inform targeted ecological management. For instance, identifying areas showing accelerated regrowth may highlight ecological hotspots for biodiversity, whereas slower recovery areas could indicate ecological stress, requiring additional restoration measures. Moreover, understanding these nuanced recovery trajectories is increasingly critical under climate-driven changes in fire regimes, providing vital information to enhance resilience through adaptive management strategies.

4.5. Comparison with Other Remote Sensing Approaches and Future Directions

While Sentinel-1 C-band SAR has demonstrated considerable potential for post-fire monitoring, especially in cloud-prone regions and open-canopy environments, its effectiveness can be limited in dense vegetation or complex terrains due to the shallow penetration depth. In contrast, L-band SAR systems such as ALOS-2 PALSAR offer deeper canopy penetration and enhanced sensitivity to biomass and vertical vegetation structure, making them more suitable for dense forests or later stages of regrowth [68–71]. Similarly, airborne LiDAR provides highly accurate structural metrics such as canopy height and leaf area index (LAI) [68,69,72], which can complement SAR data for fine-scale ecological assessments. Future research should explore multi-band SAR integration, particularly combining C-band with L-band observations (e.g., from the upcoming NASA-ISRO NISAR mission), as well as multi-source data fusion approaches that combine SAR [73,74], optical (e.g., Sentinel-2), and LiDAR datasets. These integrative strategies hold promise for improving the robustness, spatial precision, and interpretability of post-fire vegetation recovery assessments across diverse ecosystems.

4.6. Limitation and Future Work

While this study successfully demonstrates the use of Sentinel-1 SAR for post-fire monitoring, there are some limitations to consider. The reliance on unsupervised clustering may introduce some classification errors, particularly in areas with complex vegetation dynamics or mixed land cover types. Mixed pixels, where multiple land cover types occur within a single pixel, may create additional uncertainty in classification results. To address this, future studies could implement uncertainty quantification measures, such as fuzzy clustering or probabilistic classification techniques. Future research could explore the integration of supervised classification methods and advanced machine learning algorithms to enhance the accuracy of burned area mapping.

SAR imagery inherently contains speckle noise, which can obscure or distort the signal used for accurate burned area mapping and vegetation recovery assessment. Although preprocessing techniques such as smoothing filters were applied in this study to reduce speckle noise, residual speckle could still impact the clarity of classification results. Furthermore, variations in sensor geometry—including differences in incidence angles and viewing angles across image acquisitions—can result in inconsistent radar backscatter responses, complicating the interpretation of vegetation recovery trends. To address these challenges, future work could explore advanced despeckling algorithms and normalization techniques to reduce geometry-induced backscatter variability, thereby improving the accuracy and reliability of SAR-based post-fire analyses.

Additionally, increasing the frequency of temporal observations could improve the understanding of short-term vegetation recovery dynamics following fire events. The study utilised three post-fire periods, balancing data availability and computational feasibility, but higher-frequency monitoring could capture seasonal variations and regrowth trends more effectively. Incorporating L-band SAR data (e.g., ALOS-2 PALSAR), known for their deeper penetration into vegetation canopies, could significantly improve monitoring

capabilities in densely vegetated or forested regions. Future research could also explore dual-frequency SAR systems, such as the upcoming NASA-ISRO synthetic aperture radar (NISAR) mission, which will provide L- and S-band SAR data, allowing for enhanced post-fire recovery assessments.

Furthermore, integrating optical datasets (e.g., Landsat, Sentinel-2 time-series) could complement SAR observations by providing additional spectral information for vegetation regrowth analysis. High-resolution X- and C-band SAR data from commercial satellites could offer finer spatial detail, improving the monitoring of burn severity and vegetation structure changes over time.

The robustness of SAR-based analysis can be further improved through integration with SAR coherence measures or polarimetric decomposition, which offer better sensitivity to structural changes in vegetation. Field-based validation—such as measurements of canopy height, fuel load, or biomass—would also enhance confidence in interpreting SAR backscatter patterns, especially in diverse or fire-prone environments.

Finally, this study focused on a single case study within Mooloolah River National Park. Expanding the approach to other regions with diverse vegetation types, fire intensities, and climatic conditions would provide a broader validation of the methodology and assess its scalability for different ecosystems. Future work should also consider long-term post-fire monitoring to evaluate the resilience and recovery trajectories of fire-affected landscapes.

Although this study focused on heath-dominated environments in a subtropical national park, the proposed SAR-based approach holds promise for broader application in other fire-affected ecosystems such as Mediterranean shrublands, temperate forests, or savanna landscapes. However, biome-specific differences in vegetation structure, surface moisture, and fire regimes necessitate regional calibration to ensure accurate interpretation. This general framework may therefore serve as a scalable yet adaptable model for global fire recovery assessments using SAR.

5. Conclusions

This study demonstrated the effectiveness of Sentinel-1 SAR bitemporal analysis for mapping burned areas and monitoring post-fire vegetation regrowth in Mooloolah River National Park, Queensland, Australia. The results confirmed that SAR-based unsupervised classification effectively detected burn extent and regrowth trends. Key findings include the following:

- Burned area mapping: Sentinel-1 SAR successfully detected burned regions, with clear differentiation in backscatter changes corresponding to fire severity levels.
- Vegetation recovery trends: bitemporal ratios showed a progressive return to pre-fire conditions, with certain areas exhibiting enhanced regrowth by early 2023.
- Validation with optical data: dNBR analysis from Sentinel-2 confirmed fire severity patterns and supported SAR-based classifications.
- Scalability and application: the methodology is cost-effective, scalable, and adaptable for monitoring fire-affected ecosystems in different environments.

By utilising freely available SAR data and cloud-based processing in Google Earth Engine (GEE), this study presents a practical framework for continuous monitoring of fire-affected landscapes. Future research should focus on integrating field validation, exploring multi-sensor approaches, and refining classification techniques to enhance accuracy and applicability across diverse ecosystems.

This study provides a foundational framework for SAR-based post-fire monitoring in heath-dominated ecosystems. Future research should explore its application in diverse fire-prone landscapes under varying climatic regimes to assess generalizability. Emphasis should also be placed on long-term recovery monitoring, integrating SAR time-series with

ecological indicators and management objectives. Additionally, combining SAR-based workflows with emerging cloud-based platforms and automated classification methods could enable real-time decision support for post-fire ecosystem restoration and risk reduction planning.

Author Contributions: Conceptualization, H.S. and S.K.S.; methodology, H.S., P.K.S. and S.K.S.; software, S.K.S. and P.K.S.; validation, H.S. and S.K.S.; formal analysis, H.S.; investigation, H.S. and S.K.S.; resources, H.S., S.K.S. and R.P.; data curation, H.S.; writing—original draft preparation, H.S.; writing—review and editing, S.K.S., P.K.S. and R.P.; visualization, H.S. and S.K.S.; supervision, S.K.S., P.K.S. and R.P.; project administration, H.S. and S.K.S.; funding acquisition, S.K.S. All authors have read and agreed to the published version of the manuscript.

Funding: This research was supported by the University of the Sunshine Coast and the SmartSat CRC, whose activities are funded by the Australian Government's CRC Program.

Data Availability Statement: The original contributions presented in the study are included in the article, further inquiries can be directed to the corresponding author.

Acknowledgments: We thank the University of the Sunshine Coast, Queensland, Australia, for their continued academic and institutional support. This work has been supported by the SmartSat CRC, whose activities are funded by the Australian Government's CRC Program. The financial assistance provided by these entities enabled us to pursue our research objectives and complete this work. Without their support, this research would not have been possible.

Conflicts of Interest: The authors declare no conflicts of interest.

Appendix A

Google Earth Engine Code:

```
//Step 1: Define the Region of Interest (ROI)
var roi = ee.Geometry.Polygon([[
[153.0631, −26.7104],
[153.1209, −26.7106],
[153.1198, −26.7316],
[153.0668, −26.7313]
]]);

//Step 2: Load Sentinel-1 SAR Data for the Pre-Burn Period
var preFireImage = ee.ImageCollection('COPERNICUS/S1_GRD')
.filterBounds(roi)
.filterDate('xxxx-xx-xx', 'xxxx-xx-xx')//Pre-burn period
.filter(ee.Filter.listContains('transmitterReceiverPolarisation', 'VV'))
.filter(ee.Filter.eq('instrumentMode', 'IW'))
.select('VV')
.median();

//Step 3: Load Sentinel-1 SAR Data for Post-Burn Period (Multiple Time Periods for Vegetation Recovery)
//Post-burn period 1
var postFireImage1 = ee.ImageCollection('COPERNICUS/S1_GRD')
.filterBounds(roi)
.filterDate(('xxxx-xx-xx', 'xxxx-xx-xx')//Post-burn period 1
.filter(ee.Filter.listContains('transmitterReceiverPolarisation', 'VV'))
.filter(ee.Filter.eq('instrumentMode', 'IW'))
.select('VV')
.median();
```

```
//Post-burn period 2
var postFireImage2 = ee.ImageCollection('COPERNICUS/S1_GRD')
.filterBounds(roi)
.filterDate(('xxxx-xx-xx', 'xxxx-xx-xx')//Post-burn period 2
.filter(ee.Filter.listContains('transmitterReceiverPolarisation', 'VV'))
.filter(ee.Filter.eq('instrumentMode', 'IW'))
.select('VV')
.median();

//Post-burn period 3
var postFireImage3 = ee.ImageCollection('COPERNICUS/S1_GRD')
.filterBounds(roi)
.filterDate(('xxxx-xx-xx', 'xxxx-xx-xx')//Post-burn period 3
.filter(ee.Filter.listContains('transmitterReceiverPolarisation', 'VV'))
.filter(ee.Filter.eq('instrumentMode', 'IW'))
.select('VV')
.median();

//Step 4: Pre-process Data (Apply Smoothing)
var kernel = ee.Kernel.square({
radius: 9, units: 'pixels'
});

var smoothedPreFire = preFireImage.convolve(kernel);
var smoothedPostFire1 = postFireImage1.convolve(kernel);
var smoothedPostFire2 = postFireImage2.convolve(kernel);
var smoothedPostFire3 = postFireImage3.convolve(kernel);

//Step 5: Calculate Bitemporal Ratios for Each Post-Burn Period
var bitemporalRatio1 = smoothedPostFire1.divide(smoothedPreFire);//Post-burn 1 vs.
pre-burn
var bitemporalRatio2 = smoothedPostFire2.divide(smoothedPreFire);//Post-burn 2 vs.
pre-burn
var bitemporalRatio3 = smoothedPostFire3.divide(smoothedPreFire);//Post-burn 3 vs.
pre-burn

//Step 6: Display Bitemporal Ratios (to Show Vegetation Recovery)
Map.centerObject(roi, 12);
Map.addLayer(bitemporalRatio1, {min: 0.8, max: 1.2, palette: ['black', 'white']}, 'Bitemporal
Ratio (Post-Burn 1)');
Map.addLayer(bitemporalRatio2, {min: 0.8, max: 1.2, palette: ['black', 'white']}, 'Bitemporal
Ratio (Post-Burn 2)');
Map.addLayer(bitemporalRatio3, {min: 0.8, max: 1.2, palette: ['black', 'white']}, 'Bitemporal
Ratio (Post-Burn 3)');

//Step 7: Add Labels for Post-Burn Periods (Vegetation Recovery)
var labels = ['Post-Burn 1 (2021)', 'Post-Burn 2 (2022)', 'Post-Burn 3 (2023)'];
var bitemporalRatios = [bitemporalRatio1, bitemporalRatio2, bitemporalRatio3];

for (var i = 0; i < labels.length; i++) {
Map.add(ui.Label({
value: labels[i],
style: {position: 'top-right', padding: '8px'}
}));
}
```

```
//Step 8: Create and Display a Legend for the Bitemporal Ratios
var legend = ui.Panel({
style: {
position: 'bottom-left',
padding: '8px 15px'
}
});

var legendTitle = ui.Label({
value: 'Bitemporal Ratio (Grayscale)',
style: {
fontWeight: 'bold',
fontSize: '18px',
margin: '0 0 4px 0',
padding: '0'
}
});

legend.add(legendTitle);

//Define the grayscale gradient for the legend
var gradient = ui.Thumbnail({
image: ee.Image.pixelLonLat().select(0),
params: {
bbox: [0, 0, 1, 0.1],
dimensions: '100 × 20',
format: 'png',
min: 0,
max: 1,
palette: ['black', 'white']
},
style: {stretch: 'horizontal', margin: '0px 8px'}
});

legend.add(gradient);

//Add min and max labels for the gradient
var minLabel = ui.Label('0.8', {margin: '4px 8px'});
var maxLabel = ui.Label('1.2', {margin: '4px 8px', textAlign: 'right', stretch: 'horizontal'});

var legendLabels = ui.Panel({
widgets: [minLabel, maxLabel],
layout: ui.Panel.Layout.flow('horizontal')
});

legend.add(legendLabels);

//Add the legend to the map
Map.add(legend);

//Step 9: Export the Results for Further Analysis (optional)
Export.image.toDrive({
image: bitemporalRatio1,
description: 'Bitemporal_Ratio_PostBurn_1',
scale: 20,
region: roi,
fileFormat: 'GeoTIFF'
```

```
});

Export.image.toDrive({
image: bitemporalRatio2,
description: 'Bitemporal_Ratio_PostBurn_2',
scale: 20,
region: roi,
fileFormat: 'GeoTIFF'
});

Export.image.toDrive({
image: bitemporalRatio3,
description: 'Bitemporal_Ratio_PostBurn_3',
scale: 20,
region: roi,
fileFormat: 'GeoTIFF'
});
```

References

1. Keith, D.A.; Bradstock, R.A. Fire and competition in Australian heath: A conceptual model and field investigations. *J. Veg. Sci.* **1994**, *5*, 347–354. [CrossRef]
2. Lamont, B.B.; He, T.; Yan, Z. Evolutionary history of fire-stimulated resprouting, flowering, seed release and germination. *Biol. Rev.* **2019**, *94*, 903–928. [CrossRef] [PubMed]
3. Singh, H.; Srivastava, S.K. From Firestick to Satellites: Technological Advancement and Indigenous Cultural Practice in Managing Forest Fires in Australia. *Hist. Environ. Policy Pract.* **2024**, *16*, 1–24. [CrossRef]
4. Simpson, N.P.; Williams, P.A.; Mach, K.J.; Berrang-Ford, L.; Biesbroek, R.; Haasnoot, M.; Segnon, A.C.; Campbell, D.; Musah-Surugu, J.I.; Joe, E.T.; et al. Adaptation to compound climate risks: A systematic global stocktake. *iScience* **2023**, *26*, 105926. [CrossRef]
5. Fehlman, C.A.; Ryan, S.C.; Lysne, K.G.; Rundgren, Q.M.; Spurlock, T.J.; Orbison, R.O.; Runkle, J.D.; Sugg, M.M. Scoping review of the societal impacts of compound climate events. *Discov. Environ.* **2025**, *3*, 2. [CrossRef]
6. Keywood, M.; Kanakidou, M.; Stohl, A.; Dentener, F.; Grassi, G.; Meyer, C.P.; Torseth, K.; Edwards, D.; Thompson, A.M.; Lohmann, U.; et al. Fire in the Air: Biomass Burning Impacts in a Changing Climate. *Crit. Rev. Environ. Sci. Technol.* **2013**, *43*, 40–83. [CrossRef]
7. Rocca, M.E.; Brown, P.M.; MacDonald, L.H.; Carrico, C.M. Climate change impacts on fire regimes and key ecosystem services in Rocky Mountain forests. *For. Ecol. Manag.* **2014**, *327*, 290–305. [CrossRef]
8. Turner, M.G.; Donato, D.C.; Romme, W.H. Consequences of spatial heterogeneity for ecosystem services in changing forest landscapes: Priorities for future research. *Landsc. Ecol.* **2013**, *28*, 1081–1097. [CrossRef]
9. Adams, M.A. Mega-fires, tipping points and ecosystem services: Managing forests and woodlands in an uncertain future. *For. Ecol. Manag.* **2013**, *294*, 250–261. [CrossRef]
10. Ross, T.; Srivastava, S.K.; Shapcott, A. Investigating the Relationship between Fire Severity and Post-Fire Vegetation Regeneration and Subsequent Fire Vulnerability. *Forests* **2023**, *14*, 222. [CrossRef]
11. Srivastava, S.K.; Lewis, T.; Behrendorff, L.; Phinn, S. Spatial databases and techniques to assist with prescribed fire management in the south-east Queensland bioregion. *Int. J. Wildland Fire* **2021**, *30*, 90. [CrossRef]
12. Singh, H.; Ang, L.-M.; Lewis, T.; Paudyal, D.; Acuna, M.; Srivastava, P.K.; Srivastava, S.K. Trending and emerging prospects of physics-based and ML-based wildfire spread models: A comprehensive review. *J. For. Res.* **2024**, *35*, 135. [CrossRef]
13. Sos, J.; Penglase, K.; Lewis, T.; Srivastava, P.K.; Singh, H.; Srivastava, S.K. Mapping and monitoring of vegetation regeneration and fuel under major transmission power lines through image and photogrammetric analysis of drone-derived data. *Geocarto Int.* **2023**, *38*, 2280597. [CrossRef]
14. Singh, H.; Srivastava, S.K. Identification of forest fire-prone region in Lamington National Park using GIS-based multicriteria technique: Validation using field and Sentinel-2-based observations. *Geocarto Int.* **2025**, *40*, 2462484. [CrossRef]
15. Singh, S.; Singh, H.; Sharma, V.; Shrivastava, V.; Kumar, P.; Kanga, S.; Sahu, N.; Meraj, G.; Farooq, M.; Singh, S.K. Impact of forest fires on air quality in wolgan valley, new south wales, australia—A mapping and monitoring study using google earth engine. *Forests* **2022**, *13*, 4. [CrossRef]
16. Peña, M.A.; Brenning, A. Benchmarking Sentinel-2-derived predictors for long-term burn severity modelling: The 2016–2017 Chilean firestorm. *Int. J. Remote Sens.* **2023**, *44*, 2668–2690. [CrossRef]

17. Gupta, P.; Shukla, A.K.; Shukla, D.P. Sentinel 2 based burn severity mapping and assessing post-fire impacts on forests and buildings in the Mizoram, a north-eastern Himalayan region. *Remote Sens. Appl.* **2024**, *36*, 101279. [CrossRef]
18. Mallinis, G.; Mitsopoulos, I.; Chrysafi, I. Evaluating and comparing Sentinel 2A and Landsat-8 Operational Land Imager (OLI) spectral indices for estimating fire severity in a Mediterranean pine ecosystem of Greece. *Gisci. Remote Sens.* **2018**, *55*, 1–18. [CrossRef]
19. Alcaras, E.; Costantino, D.; Guastaferro, F.; Parente, C.; Pepe, M. Normalized Burn Ratio Plus (NBR+): A New Index for Sentinel-2 Imagery. *Remote Sens.* **2022**, *14*, 1727. [CrossRef]
20. Kurbanov, E.; Vorobev, O.; Lezhnin, S.; Sha, J.; Wang, J.; Li, X.; Cole, J.; Dergunov, D.; Wang, Y. Remote sensing of forest burnt area, burn severity, and post-fire recovery: A review. *Remote Sens.* **2022**, *14*, 4714. [CrossRef]
21. Gibson, R.; Danaher, T.; Hehir, W.; Collins, L. A remote sensing approach to mapping fire severity in south-eastern Australia using sentinel 2 and random forest. *Remote Sens. Environ.* **2020**, *240*, 111702. [CrossRef]
22. Yang, S.; Huang, Q.; Yu, M. Advancements in remote sensing for active fire detection: A review of datasets and methods. *Sci. Total Environ.* **2024**, *943*, 173273. [CrossRef] [PubMed]
23. Singh, H.; Pandey, A.C. Land deformation monitoring using optical remote sensing and PS-InSAR technique nearby Gangotri glacier in higher Himalayas. *Model Earth Syst. Environ.* **2021**, *7*, 221–233. [CrossRef]
24. Bauer-Marschallinger, B.; Freeman, V.; Cao, S.; Paulik, C.; Schaufler, S.; Stachl, T.; Modanesi, S.; Massari, C.; Ciabatta, L.; Brocca, L.; et al. Toward Global Soil Moisture Monitoring with Sentinel-1: Harnessing Assets and Overcoming Obstacles. *IEEE Trans. Geosci. Remote Sens.* **2019**, *57*, 520–539. [CrossRef]
25. Torres, R.; Snoeij, P.; Geudtner, D.; Bibby, D.; Davidson, M.; Attema, E.; Potin, P.; Rommen, B.; Floury, N.; Brown, M.; et al. GMES Sentinel-1 mission. *Remote Sens. Environ.* **2012**, *120*, 9–24. [CrossRef]
26. Paluba, D.; Papale, L.G.; Laštovička, J.; Perivolioti, T.-M.; Kalaitzis, P.; Mouratidis, A.; Karadimou, G.; Štych, P. Tracking burned area progression in an unsupervised manner using Sentinel-1 SAR data in Google Earth Engine. *IEEE J. Sel. Top. Appl. Earth Obs. Remote Sens.* **2024**, *17*, 15612–15634. [CrossRef]
27. Addison, P.; Oommen, T. Utilizing satellite radar remote sensing for burn severity estimation. *Int. J. Appl. Earth Obs. Geoinf.* **2018**, *73*, 292–299. [CrossRef]
28. Imperatore, P.; Azar, R.; Calo, F.; Stroppiana, D.; Brivio, P.A.; Lanari, R.; Pepe, A. Effect of the Vegetation Fire on Backscattering: An Investigation Based on Sentinel-1 Observations. *IEEE J. Sel. Top. Appl. Earth Obs. Remote Sens.* **2017**, *10*, 4478–4492. [CrossRef]
29. Yi, Y.; Chen, R.H.; Moghaddam, M.; Kimball, J.S.; Jones, B.M.; Jandt, R.R.; Miller, E.A.; Miller, C.E. Sensitivity of Multifrequency Polarimetric SAR Data to Postfire Permafrost Changes and Recovery Processes in Arctic Tundra. *IEEE Trans. Geosci. Remote Sens.* **2022**, *60*, 1–15. [CrossRef]
30. Saatchi, S.S.; Houghton, R.A.; Alvalá, R.C.D.S.; Soares, J.V.; Yu, Y. Distribution of aboveground live biomass in the Amazon basin. *Glob. Change Biol.* **2007**, *13*, 816–837. [CrossRef]
31. Santoro, M.; Cartus, O.; Antropov, O.; Miettinen, J. Estimation of Forest Growing Stock Volume with Synthetic Aperture Radar: A Comparison of Model-Fitting Methods. *Remote Sens.* **2024**, *16*, 4079. [CrossRef]
32. Santoro, M.; Cartus, O.; Fransson, J.E.; Shvidenko, A.; McCallum, I.; Hall, R.J.; Beaudoin, A.; Beer, C.; Schmullius, C. Estimates of Forest Growing Stock Volume for Sweden, Central Siberia, and Québec Using Envisat Advanced Synthetic Aperture Radar Backscatter Data. *Remote Sens.* **2013**, *5*, 4503–4532. [CrossRef]
33. Marchese, F.; Mazzeo, G.; Filizzola, C.; Coviello, I.; Falconieri, A.; Lacava, T.; Paciello, R.; Pergola, N.; Tramutoli, V. Issues and Possible Improvements in Winter Fires Detection by Satellite Radiances Analysis: Lesson Learned in Two Regions of Northern Italy. *IEEE J. Sel. Top. Appl. Earth Obs. Remote Sens.* **2017**, *10*, 3297–3313. [CrossRef]
34. Katagis, T.; Polychronaki, A.; Gitas, I.Z. Mapping burned areas and assessing short-term fire effects with the use of object-based analysis and high resolution satellite imagery. In *Remote Sensing for a Changing Europe*; IOS Press: Amsterdam, The Nertherlands, 2009. [CrossRef]
35. Lasko, K.; Vadrevu, K.P.; Tran, V.T.; Justice, C. Mapping Double and Single Crop Paddy Rice with Sentinel-1A at Varying Spatial Scales and Polarizations in Hanoi, Vietnam. *IEEE J. Sel. Top. Appl. Earth Obs. Remote Sens.* **2018**, *11*, 498–512. [CrossRef]
36. Dalponte, M.; Solano-Correa, Y.T.; Marinelli, D.; Liu, S.; Yokoya, N.; Gianelle, D. Detection of forest windthrows with bitemporal COSMO-SkyMed and Sentinel-1 SAR data. *Remote Sens. Environ.* **2023**, *297*, 113787. [CrossRef]
37. Hu, X.; Li, L.; Huang, J.; Zeng, Y.; Zhang, S.; Su, Y.; Hong, Y.; Hong, Z. Radar vegetation indices for monitoring surface vegetation: Developments, challenges, and trends. *Sci. Total Environ.* **2024**, *945*, 173974. [CrossRef]
38. Hylander, K.; Frisk, C.A.; Nemomissa, S.; Johansson, M.U. Rapid post-fire re-assembly of species-rich bryophyte communities in Afroalpine heathlands. *J. Veg. Sci.* **2021**, *32*, e13033. [CrossRef]
39. Rainsford, F.W.; Kelly, L.T.; Leonard, S.W.J.; Bennett, A.F. Fire and functional traits: Using functional groups of birds and plants to guide management in a fire-prone, heathy woodland ecosystem. *Divers. Distrib.* **2022**, *28*, 372–385. [CrossRef]
40. Velle, L.G.; Nilsen, L.S.; Vandvik, V. The age of Calluna stands moderates post-fire regeneration rate and trends in northern *Calluna* heathlands. *Appl. Veg. Sci.* **2012**, *15*, 119–128. [CrossRef]

41. Lindenmayer, D.; Burns, E.; Thurgate, N.I.Y.; Lowe, A.J. *Biodiversity and Environmental Change: Monitoring, Challenges and Direction*; CSIRO Publishing: Clayton, Australia, 2014; Volume 213.
42. Tariq, A.; Shu, H.; Li, Q.; Altan, O.; Khan, M.R.; Baqa, M.F.; Lu, L. Quantitative Analysis of Forest Fires in Southeastern Australia Using SAR Data. *Remote Sens.* **2021**, *13*, 2386. [CrossRef]
43. Tanase, M.; de la Riva, J.; Santoro, M.; Pérez-Cabello, F.; Kasischke, E. Sensitivity of SAR data to post-fire forest regrowth in Mediterranean and boreal forests. *Remote Sens. Environ.* **2011**, *115*, 2075–2085. [CrossRef]
44. De Luca, G.; Silva, J.M.N.; Modica, G. Short-term temporal and spatial analysis for post-fire vegetation regrowth characterization and mapping in a Mediterranean ecosystem using optical and SAR image time-series. *Geocarto Int.* **2022**, *37*, 15428–15462. [CrossRef]
45. Ghosh, S.; Kumar, D.; Kumari, R. Cloud-based large-scale data retrieval, mapping, and analysis for land monitoring applications with Google Earth Engine (GEE). *Environ. Chall.* **2022**, *9*, 100605. [CrossRef]
46. Amani, M.; Ghorbanian, A.; Ahmadi, S.A.; Kakooei, M.; Moghimi, A.; Mirmazloumi, S.M.; Moghaddam, S.H.A.; Mahdavi, S.; Ghahremanloo, M.; Parsian, S.; et al. Google Earth Engine Cloud Computing Platform for Remote Sensing Big Data Applications: A Comprehensive Review. *IEEE J. Sel. Top. Appl. Earth Obs. Remote Sens.* **2020**, *13*, 5326–5350. [CrossRef]
47. Hrysiewicz, A.; Holohan, E.P.; Donohue, S.; Cushnan, H. SAR and InSAR data linked to soil moisture changes on a temperate raised peatland subjected to a wildfire. *Remote Sens. Environ.* **2023**, *291*, 113516. [CrossRef]
48. Chuvieco, E.; Aguado, I.; Salas, J.; García, M.; Yebra, M.; Oliva, P. Satellite Remote Sensing Contributions to Wildland Fire Science and Management. *Curr. For. Rep.* **2020**, *6*, 81–96. [CrossRef]
49. Parker, A.L.; Castellazzi, P.; Fuhrmann, T.; Garthwaite, M.C.; Featherstone, W.E. Applications of Satellite Radar Imagery for Hazard Monitoring: Insights from Australia. *Remote Sens.* **2021**, *13*, 1422. [CrossRef]
50. De Petris, S.; Momo, E.J.; Sarvia, F.; Borgogno-Mondino, E. Multitemporal dual-pol Sentinel-1 data to support monitoring of forest post-fire dynamics. *Geocarto Int.* **2022**, *37*, 15463–15484. [CrossRef]
51. Singh, H.; Ang, L.-M.; Srivastava, S.K. Benchmarking Artificial Neural Networks and U-Net Convolutional Architectures for Wildfire Susceptibility Prediction: Innovations in Geospatial Intelligence. *IEEE Trans. Geosci. Remote Sens.* **2025**, *63*, 1–15. [CrossRef]
52. Singh, H.; Ang, L.-M.; Srivastava, S.K. Active wildfire detection via satellite imagery and machine learning: An empirical investigation of Australian wildfires. *Nat. Hazards* **2025**, *21*, 9777–9800. [CrossRef]
53. Department of Environment and Science, Queensland Government. *Mooloolah River National Park Management Plan*; Queensland Government: Brisbane, Australia, 1999. Available online: https://parks.desi.qld.gov.au/__data/assets/pdf_file/0037/167797/mooloolah-river-national-park-2000.pdf (accessed on 10 June 2025).
54. Department of the Environment and Energy. NVIS Fact Sheet MVG 18—Heathlands. Australian Government, Canberra, Australia. Available online: https://www.agriculture.gov.au/sites/default/files/documents/mvg18-nvis-heathlands.pdf (accessed on 10 June 2025).
55. Lamont, B.B.; Keith, D.A. Heathlands and Associated Shrublands. In *Australian Vegetation*, 3rd ed.; Cambridge University Press: Cambridge, UK, 2017; Chapter 14, pp. 339–367.
56. Ygorra, B.; Frappart, F.; Wigneron, J.; Moisy, C.; Catry, T.; Baup, F.; Hamunyela, E.; Riazanoff, S. Monitoring loss of tropical forest cover from Sentinel-1 time-series: A CuSum-based approach. *Int. J. Appl. Earth Obs. Geoinf.* **2021**, *103*, 102532. [CrossRef]
57. Steele, J.G. *Aboriginal Pathways: In Southeast Queensland and the Richmond River*; University of Queensland Press: Brisbane, Australia, 2015.
58. Wei, J.; Zhang, Y.; Wu, H.; Cui, B. The Automatic Detection of Fire Scar in Alaska using Multi-Temporal PALSAR Polarimetric SAR Data. *Can. J. Remote Sens.* **2018**, *44*, 447–461. [CrossRef]
59. Fahim, A. K and starting means for k-means algorithm. *J. Comput. Sci.* **2021**, *55*, 101445. [CrossRef]
60. Ikotun, A.M.; Ezugwu, A.E.; Abualigah, L.; Abuhaija, B.; Heming, J. K-means clustering algorithms: A comprehensive review, variants analysis, and advances in the era of big data. *Inf. Sci.* **2023**, *622*, 178–210. [CrossRef]
61. Jimeno-Llorente, L.; Marcos, E.; Fernández-Guisuraga, J.M. The Effects of Fire Severity on Vegetation Structural Complexity Assessed Using SAR Data Are Modulated by Plant Community Types in Mediterranean Fire-Prone Ecosystems. *Fire* **2023**, *6*, 450. [CrossRef]
62. Zhou, Z.; Liu, L.; Jiang, L.; Feng, W.; Samsonov, S.V. Using Long-Term SAR Backscatter Data to Monitor Post-Fire Vegetation Recovery in Tundra Environment. *Remote Sens.* **2019**, *11*, 2230. [CrossRef]
63. Moran, M.S. Principles and Applications of Imaging Radar, Manual of Remote Sensing, 3rd Edition, Volume 2. *Eos Trans. Am. Geophys. Union* **1999**, *80*, 67. [CrossRef]
64. Ulaby, F.T.; Moore, R.K.; Fung, A.K. *Microwave Remote Sensing: Active and Passive*; Artech House: Norwood, MA, USA, 1986; Volume 3.

65. Fernández-Guisuraga, J.M.; Marcos, E.; Suárez-Seoane, S.; Calvo, L. ALOS-2 L-band SAR backscatter data improves the estimation and temporal transferability of wildfire effects on soil properties under different post-fire vegetation responses. *Sci. Total Environ.* **2022**, *842*, 156852. [CrossRef]
66. De Luca, G.; Silva, J.M.N.; Modica, G. A workflow based on Sentinel-1 SAR data and open-source algorithms for unsupervised burned area detection in Mediterranean ecosystems. *Gisci. Remote Sens.* **2021**, *58*, 516–541. [CrossRef]
67. Stroppiana, D.; Azar, R.; Calò, F.; Pepe, A.; Imperatore, P.; Boschetti, M.; Silva, J.M.N.; Brivio, P.A.; Lanari, R. Integration of Optical and SAR Data for Burned Area Mapping in Mediterranean Regions. *Remote Sens.* **2015**, *7*, 1320–1345. [CrossRef]
68. Pereira, E.A.V.; Martínez, M.A.V.; Gómez, F.J.R.; Navarro-Cerrillo, R.M. Temporal Changes in Mediterranean Pine Forest Biomass Using Synergy Models of ALOS PALSAR-Sentinel 1-Landsat 8 Sensors. *Remote Sens.* **2023**, *15*, 3430. [CrossRef]
69. Ottinger, M.; Kuenzer, C. Spaceborne L-Band Synthetic Aperture Radar Data for Geoscientific Analyses in Coastal Land Applications: A Review. *Remote Sens.* **2020**, *12*, 2228. [CrossRef]
70. Koyama, C.N.; Shimada, M.; Ohki, M.; Tadono, T. From ALOS-2 to ALOS-4: Japan's pioneering L-band SARs for global vegetation monitoring: State-of-the-art and future perspectives. In *Sensors, Systems, and Next-Generation Satellites XXVII*; Kimura, T., Babu, S.R., Hélière, A., Eds.; SPIE: Amsterdam, The Netherlands, 2023; p. 16. [CrossRef]
71. Padalia, H.; Prakash, A.; Watham, T. Modelling aboveground biomass of a multistage managed forest through synergistic use of Landsat-OLI, ALOS-2 L-band SAR and GEDI metrics. *Ecol. Inform.* **2023**, *77*, 102234. [CrossRef]
72. Hopkinson, C.; Lovell, J.; Chasmer, L.; Jupp, D.; Kljun, N.; van Gorsel, E. Integrating terrestrial and airborne lidar to calibrate a 3D canopy model of effective leaf area index. *Remote Sens. Environ.* **2013**, *136*, 301–314. [CrossRef]
73. Hashemi, M.G.Z.; Jalilvand, E.; Alemohammad, H.; Tan, P.-N.; Das, N.N. Review of synthetic aperture radar with deep learning in agricultural applications. *ISPRS J. Photogramm. Remote Sens.* **2024**, *218*, 20–49. [CrossRef]
74. Kalecinski, N.I.; Skakun, S.; Torbick, N.; Huang, X.; Franch, B.; Roger, J.-C.; Vermote, E. Crop yield estimation at different growing stages using a synergy of SAR and optical remote sensing data. *Sci. Remote Sens.* **2024**, *10*, 100153. [CrossRef]